

# Challenges and Opportunities in High-dimensional Variational Inference

**Akash Kumar Dhaka\***

**Alejandro Catalina\***

*Department of Computer Science*

*Aalto University*

*00076 Aalto, Finland*

AKASH.DHAKA@AALTO.FI

ALEJANDRO.CATALINA@AALTO.FI

**Manushi Welandawe**

**Jonathan Huggins**

*Department of Mathematics & Statistics*

*Boston University, USA*

MANUSHIW@BU.EDU

HUGGINS@BU.EDU

**Michael Riis Andersen**

*DTU Compute*

*Technical University of Denmark*

*Denmark*

MIRI@DTU.DK

**Aki Vehtari**

*Department of Computer Science*

*Aalto University*

*00076 Aalto, Finland*

AKI.VEHTARI@AALTO.FI

## Abstract

We explore the limitations of and best practices for using black-box variational inference to estimate posterior summaries of the model parameters. By taking an importance sampling perspective, we are able to explain and empirically demonstrate: 1) why the intuitions about the behavior of approximate families and divergences for low-dimensional posteriors fail for higher-dimensional posteriors, 2) how we can diagnose the pre-asymptotic reliability of variational inference in practice by examining the behavior of the density ratios (i.e., importance weights), 3) why the choice of variational objective is not as relevant for higher-dimensional posteriors, and 4) why, although flexible variational families can provide some benefits in higher dimensions, they also introduce additional optimization challenges. Based on these findings, for high-dimensional posteriors we recommend using the exclusive KL divergence that is most stable and easiest to optimize, and then focusing on improving the variational family or using model parameter transformations to make the posterior more similar to the approximating family. Our results also show that in low to moderate dimensions, heavy-tailed variational families and mass-covering divergences can increase the chances that the approximation can be improved by importance sampling.

---

\*. Equal contribution.

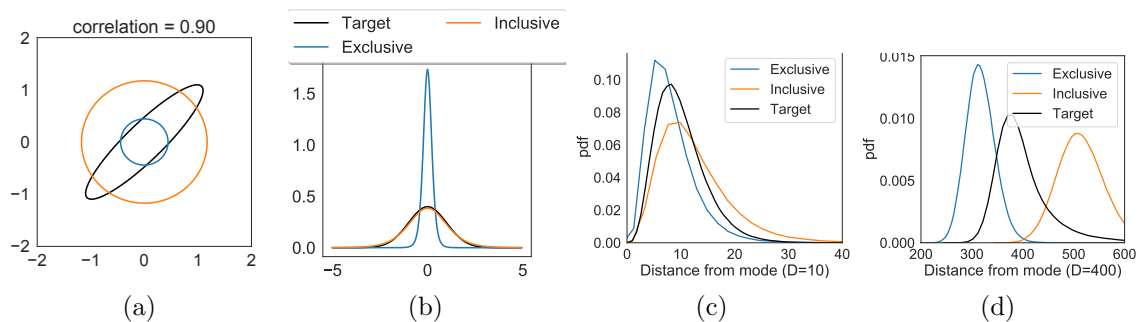


Figure 1: Illustration of a mean-field approximation with exclusive (mode-seeking) and inclusive (mass-covering) divergences. The target is a normal distribution and the approximate distribution is a  $t$  distribution with 7 degrees of freedom. **(a)** The typical 2D illustration (correlation 0.9) gives impression that the inclusive divergence would provide a better approximation. **(b)** The marginal distribution of the 2D illustration, showing the heavier tails of the approximate distribution. Heavier tails guarantee that the importance ratios are bounded, and thus the importance sampling estimate has asymptotically finite variance. **(c,d)** The marginal densities as a function of the distance from the mode in 10- and 400-dimensional examples (correlation 0.10). These demonstrate that, even for much lower correlation levels, the intuition from the low-dimensional examples does not carry over to higher dimensions: although the importance ratios are still bounded and importance sampling has asymptotically finite variance, the overlap in typical sets of the target and the approximations gets worse both for exclusive and inclusive divergences.

## 1. Introduction

A great deal of progress has been made in black box variational inference (BBVI) methods for Bayesian posterior approximations, but the interplay between the approximating family, divergence measure, gradient estimators and stochastic optimizer is non-trivial – and even more so for high-dimensional posteriors (Wang et al., 2018; Yao et al., 2018; Geffner and Domke, 2020a; Agrawal et al., 2020). While the main focus in the machine learning literature has been on improving predictive accuracy, the choice of method components becomes even more critical when the goal is to obtain accurate summaries of the posterior itself.

In this paper, we show that, while the choice of approximating family and divergence is often motivated by low-dimensional illustrations, the intuition from these examples do not necessarily carry over to higher-dimensional settings. In higher dimensions, even over-dispersed distributions miss the typical set of the target (MacKay, 2003; Vehtari et al., 2019). Thus, as illustrated in Fig. 1, the benefits of heavy-tailed approximate families and divergences favoring mass-covering diminish. Moreover, we should expect that, in higher dimensions, estimation of (the gradients of) many commonly used divergences may be infeasible when the variational family is a poor match for the target distribution. And, even if we had access to asymptotically unbiased and finite-variance estimates of the divergence, the estimator variance may be so large that reaching the asymptotic regime would require an infeasible amount of computation, with the pre-asymptotic behavior exhibiting large biases and near-zero convergence rate.

To better explain and empirically validate these issues, draw on connections between the estimation of common divergences using Black-box variational inference and importance sampling are strong: use Monte Carlo estimates of expectations of functions involving the density ratio between the target and the approximate distribution.

The importance sampling perspective is helpful both when analysing the variability of divergence and gradient estimates, and when using the variational posterior approximation as an importance sampling proposal distribution (Geweke, 1989). As the dimensionality grows, importance sampling encounters the same challenge as computation of the divergences – that is, it is more likely that the typical set of the approximation and the target do not overlap sufficiently, and the required sampled size for more accurate estimates grows exponentially with the KL divergence (Chatterjee and Diaconis, 2018).

We use the Pareto  $k$  diagnostic (Vehtari et al., 2019) as a simple and practical approach for estimating both the required minimal sample size and obtaining empirical and conceptual insights into pre-asymptotic convergence rate estimators of common divergences and their gradients. We demonstrate how the estimated Pareto  $k$  rapidly increases as the dimensionality grows, regardless of the approximate family and divergence measure optimised. We thoroughly study the impact of the choice of divergence measures when the dimensionality of the model grows. We consider the exclusive and inclusive Kullback–Leibler (KL) divergences (Bornschein and Bengio, 2015; Naesseth et al., 2020), tail-adaptive  $f$ -divergence Wang et al. (2018),  $\chi^2$  divergence (Dieng et al., 2017), and  $\alpha$ -divergences (Hernandez-Lobato et al., 2016), and the resulting variational approximation for isotropic Gaussian and Student- $t$  and normalising flow families.

Our main contributions are: 1) we identify and discuss the main challenges in optimizing a variational objective in higher dimensional cases for different divergences and approximating families, 2) we demonstrate the use of the Pareto  $k$  diagnostic for discovering divergence and gradient estimation problems, and for estimating the minimal Monte Carlo sample size requirement, 3) we provide an extensive empirical study using simulated and several commonly used real datasets with both Gaussian and non-Gaussian target distributions, and 4) based on our analyses and results, we provide justified recommendations on design choices for different scenarios, including low- to moderate-dimensional and high-dimensional posteriors.

## 2. Preliminaries and Background

Let  $p(\theta, Y)$  be a joint distribution of a probabilistic model, where  $\theta \in \mathbb{R}^D$  is a vector of model parameters and  $Y$  is the observed data. In Bayesian analysis, the posterior  $p(\theta) := p(\theta | Y) \propto p(Y|\theta)p_0(\theta)$  is typically the object of interest, but most posterior summaries of interest are not accessible because the normalizing integral, in general, is intractable. Variational inference approximates the exact posterior  $p(\theta | Y)$  using a distribution  $q \in \mathcal{Q}$  from a family of tractable distributions  $\mathcal{Q}$ . The best approximation is determined by minimizing a divergence  $D(p \parallel q)$ , which measures the discrepancy between  $p$  and  $q$ :

$$q_{\lambda^*} = \arg \min_{q_{\lambda} \in \mathcal{Q}} D(p \parallel q), \quad (1)$$

where  $\lambda \in \mathbb{R}^K$  is a vector parameterizing the variational family  $\mathcal{Q}$ . Thus, the properties of the resulting approximation  $q$  are determined by the choice of variational family  $\mathcal{Q}$  as well as the choice of divergence  $D$ .

The family  $\mathcal{Q}$  is often chosen such that quantities of interest (e.g., moments of  $q$ ) can be computed efficiently. For example,  $q$  can be used to compute Monte Carlo or importance sampling estimates of the quantities of interest. Let  $w(\theta) := p(\theta, Y)/q(\theta)$  denote the density ratio between the joint and approximate distributions. For a function  $\phi : \mathbb{R}^D \rightarrow \mathbb{R}$ , the *self-normalized importance sampling estimator* for the posterior expectation  $\mathbb{E}_{\theta \sim p}[\phi(\theta)]$  is given by

$$\hat{I}(\phi) := \sum_{s=1}^S \frac{w(\theta_s)}{\sum_{s'=1}^S w(\theta_{s'})} \phi(\theta_s),$$

where  $\theta_1, \dots, \theta_S \sim q$  are independent. Using importance sampling can allow for computation of more accurate posterior summaries and to go beyond the limitations of the variational family. For example, it makes it possible to estimate the posterior covariance even when using a mean-field variational family. Pareto smoothed importance sampling (PSIS) can be used to stabilize the importance sampling estimates (Vehtari et al., 2019).

## 2.1 Variational families

Let  $q_\lambda(\theta)$  be an approximating family parameterised by a  $K$ -dimensional vector  $\lambda \in \mathbb{R}^K$  for  $D$ -dimensional inputs  $\theta \in \mathbb{R}^D$ . Typical choices of  $q$  include mean-field Gaussian and Student’s  $t$  families (Blei et al., 2017; Huggins et al., 2020), full and low rank Gaussians (Ong et al., 2018; Kucukelbir et al., 2015), mixtures of exponential families (Lin et al., 2019; Miller et al., 2017), and normalising flows (Rezende and Mohamed, 2015). We focus on the most popular mean-field and normalizing flow families.

Mean-field families assume independence across the  $D$  dimensions:  $q(\theta) = \prod_{i=1}^D q_i(\theta_i)$ , where each  $q_i$  typically belongs to some exponential family or other simple class of distributions.

Normalising flows provide more flexible families that can capture correlation and non-linear dependencies. A normalizing flow is defined via the transformation of a probability density through a sequence of invertible mappings. By repeatedly applying the change of variables, the initial density *flows* through the sequence of transformations (Rezende and Mohamed, 2015).

By composing several maps, a simple distribution such as a mean-field Gaussian can be transformed into a more complex one. Here we use planar flows (Rezende and Mohamed, 2015) and non-volume preserving (NVP) flows (Dinh et al., 2017).

## 2.2 $f$ -divergences and stochastic optimization

The most commonly used divergences are examples of  $f$ -divergences (Wan et al., 2020).

For a convex function  $f$  satisfying  $f(1) = 0$ , the  $f$ -divergence is given by

$$D_f(p \parallel q) := \mathbb{E}_{\theta \sim q} \left[ f \left( \frac{p(\theta \mid Y)}{q(\theta)} \right) \right].$$

The exclusive Kullback–Leibler (KL) divergence corresponds to  $f(w) = -\log(w)$ , the inclusive KL divergence corresponds to  $f(w) = w \log(w)$ , the  $\chi^2$  divergence corresponds to



$f(w) = w^2/2$  and, finally, general  $\alpha$ -divergences correspond to  $(w^\alpha - w)/\alpha(\alpha - 1)$ . We also consider the *adaptive*  $f$ -divergence proposed by Wang et al. (2018).

It has been established in numerous special cases that minimizing the  $f$ -divergence is equivalent to minimizing the loss function

$$\mathcal{L}_f(p \parallel q) := \mathbb{E}_{\theta \sim q}[f(w(\theta))]. \quad (2)$$

(Although see Wan et al. (2020) for a different approach.) Let  $L(\lambda) := \mathcal{L}_f(p \parallel q_\lambda)$  denote the loss as a function of the variational parameters  $\lambda$ . Many commonly used objectives such as the ELBO (Bishop, 2006) and CUBO (Dieng et al., 2017) can also be formulated this way. The loss and its gradient can both be approximated using, respectively, the Monte Carlo estimates

$$\hat{L}(\lambda) = \frac{1}{S} \sum_{s=1}^S f(w(\theta_s)) \quad \text{and} \quad \hat{G}(\lambda) = \frac{1}{S} \sum_{s=1}^S g(\theta_s), \quad (3)$$

where  $\theta_1, \dots, \theta_S$  are independent draws from  $q_\lambda$  and  $g : \mathbb{R}^K \rightarrow \mathbb{R}^K$  is an appropriate gradient-like function that depends on  $f$  and  $w$ . In the case of the adaptive  $f$ -divergence, the importance weights  $w(\theta_1), \dots, w(\theta_S)$  are sorted, and the gradients corresponding to each sample are then weighed by the empirical rank.

The gradient estimates can be used in a stochastic gradient descent scheme such that

$$\lambda^{t+1} \leftarrow \lambda^t + \eta_t \hat{G}(\lambda^t), \quad (4)$$

where  $\eta_t$  is the step size. In practice, more stable adaptive stochastic gradient optimisation methods such as RMSProp or Adam (Duchi et al., 2011; Hinton and Tieleman, 2012), which smooth or normalize the noisy gradients, are used.

### 2.3 Gradient estimators

Stable and low-variance gradient estimators are central for solving the stochastic optimization problem efficiently with high accuracy. The two most popular gradient estimators in the literature are the score function and the reparameterised gradient estimator (Mohamed et al., 2019; Xu et al., 2019).

**Score function.** The score function gradient for the loss in Eq. (2) corresponds to  $\hat{G}(\lambda)$  with  $g(\theta) = \{f(w(\theta)) - w(\theta)f'(w(\theta))\}\nabla_\lambda \log q_\lambda(\theta)$ . It is a general-purpose estimator that applies to both discrete and continuous distributions  $q$ , but it is known to suffer from high variance.

This estimator is used for the *mass-covering* divergences such as the inclusive KL and general  $\alpha$ -divergences with  $\alpha > 1$ . For these divergences the importance weights must be replaced with self-normalized importance weights  $w(\theta_s)/\sum_{i=1}^S w(\theta_i)$ , which leads to an asymptotically unbiased estimate, but introduces a finite sample size bias of  $\mathcal{O}(1/S)$ .

#### Reparameterization gradients.

The reparameterization gradient (Mohamed et al., 2019) works by expressing the distribution  $q$  as a deterministic transformation of a simpler base distribution  $r$  such that  $T_\lambda(\epsilon) \sim q_\lambda$  with  $\epsilon \sim r$ . This allows writing an expectation with respect to  $q$  as an expectation over the simpler distribution  $r$ . The reparameterization estimator for Eq. (2) corresponds to

$\hat{G}(\lambda)$  but with  $g(\epsilon_s) = \nabla_\lambda f(w(T_\lambda(\epsilon_s)))$  (for  $\epsilon_s \sim r$ ) in place of  $g(\theta)$ , noting that  $w$  implicitly depend on  $\lambda$  as well.

Unlike the score function approach, the reparameterization gradient uses the derivative of the log joint density through  $w$ , which can lead to lower-variance gradient estimates.

A variant of the reparameterised gradient estimator is the path gradient (or “sticking the landing”) estimator (Mohamed et al., 2019; Roeder et al., 2018). We will not consider it in detail because, while the path gradient has lower variance when  $q$  is close to  $p$ , it can have much larger variance when  $q$  is a poor approximation to  $p$  – which will be the typical situation in our experiments.

### 3. Pre-asymptotic Reliability of Variational Inference

In this section, we study what is required to obtain reliable estimates of the variational divergence and optimal variational approximation. As we have seen, the most common variational divergences and their Monte Carlo gradient estimators can be expressed in terms of the density ratio  $w(\theta)$ . Since accurate optimization requires low-variance and (nearly) unbiased gradient estimates, reliable black-box variational inference ultimately depends on the behavior of  $w(\theta)$ . Moreover, determining convergence and validating the quality of variational approximations can require accurate estimates of variational divergences (Kucukelbir et al., 2015; Huggins et al., 2020).

While *asymptotically* (in the number of iterations and Monte Carlo sample size  $S$ ) there may be no issues with stochastic optimization or divergence estimation, in practice black-box variational inference operates in the *pre-asymptotic* regime.

**Density ratios and the central limit theorem.** Recall that the variational loss  $\mathcal{L}_f(p \parallel q_\lambda)$  is defined in terms of a convex function  $f(w)$  of the density ratio  $w(\theta)$ . These weights can also be interpreted as importance sampling weights, where the proposal distribution is the variational family  $q_\lambda(\theta)$ .

The relationship between importance sampling and variational inference has been discussed, for instance, by Li and Turner (2016); Wang et al. (2018) and Bamler et al. (2017). The stability and convergence of the stochastic optimization process and the accuracy of the objective estimates depend on the properties of Monte Carlo estimates  $\hat{G}(\lambda)$  and  $\hat{L}(\lambda)$ . These estimates depend in turn on the distribution of  $w(\theta_s)$  for draws  $\theta_s \sim q_\lambda$ . Even if these Monte Carlo estimates are designed to be unbiased or asymptotically unbiased, the distribution of  $w$  can be extremely heavy-tailed. Consequently, the distributions of  $g(\theta_s)$  and  $f(w(\theta_s))$  are also likely to be heavy-tailed. In such cases, the Monte Carlo estimate is often dominated by a small number of weights  $w(\theta_s)$ . In practice, this means that the variance of some of these estimates may be infinite or extremely large, implying that the central limit theorem (CLT) does not apply (Chen and Shao, 2004) or the pre-asymptotic constant for the CLT is so big that the pre-asymptotic convergence is extremely slow (Vehtari et al., 2019). Moreover, in practice even unbiased estimates may typically be biased because of the skewness of the distribution of  $f(w(\theta_s))$ .

#### Characterizing pre-asymptotic behavior.

In light of potentially heavy-tailed  $w(\theta)$ , it is important to verify the pre-asymptotic behavior of the Monte Carlo estimators used in variational inference. We follow the approach

Table 1: Required finite moments to estimate divergences, for  $\delta > 0$  and  $\alpha > 1$  (Epifani et al., 2008, Table 2).

Objective	$f(w)$	Moments
Exclusive KL	$\log(w)$	$\delta$
Inclusive KL	$w \log(w)$	$2 + \delta$
$\chi^2$	$(w^2 - w)/2$	4
$\alpha$ -divergence	$(w^\alpha - w)/(\alpha(\alpha - 1))$	$2\alpha$

of Vehtari et al. (2019), which propose to estimate the *tail index*

$$k := \inf \left\{ k' > 0 : \mathbb{E}_{\theta \sim q} \{w(\theta)\}^{\frac{1}{k'}} < \infty \right\}. \quad (5)$$

The integer  $\lfloor 1/k \rfloor$  indicates the number of finite moments. For example, the variance of the distribution is finite if  $k < \frac{1}{2}$ . An empirical estimate  $\hat{k}$  can be obtained by fitting a generalized Pareto distribution to the observed tail draws. Vehtari et al. (2019) show that the minimal sample size to have a small error with high probability scales as

$$S = \mathcal{O} \left( \exp \{k/(1 - k)^2\} \right). \quad (6)$$

Vehtari et al. (2019) also demonstrate that  $\hat{k}$  provides a practical *pre-asymptotic convergence rate estimate* even when the variance is infinite and a generalized CLT holds. While estimating  $\hat{k}$  in general requires larger sample size than is commonly used to estimate the stochastic gradients, we can still use it to diagnose and identify the challenges with different divergences. If  $\hat{k} > 0.7$ , the minimal sample size to obtain a reliable Monte Carlo estimate is so large that it is usually infeasible in practice.

**Required moments to estimate each divergence.** The required number of finite moments (or moments that can be reliably estimated with a feasible Monte Carlo sample size) to estimate a quantity of interest depends on its relationship with the density ratios  $w(\theta)$ .

The tail index is helpful for recognizing how challenging the different divergences are. For example, if  $k < \frac{1}{2}$  for the distribution of  $w$ , then the CLT holds for the expectation of  $w$ . But the  $\chi^2$ -divergence requires the expectation of  $w^2$ , which then requires  $k < \frac{1}{4}$  for the distribution of  $w$  for the CLT to hold. On the other hand, the distribution of  $\log(w)$  tends to have a much lighter tail than the distribution of  $w$ , so Monte Carlo estimates of its expectation are in general more stable. In Table 1 we show a summary of the divergences we study in our work and the required number of finite moments for each of them. The faster  $f(w)$  increases as  $w$  increase, the more finite moments that are required – which only get harder to estimate in high-dimensional cases.

**Gradient estimators.** The form of  $f(w)$  also affects the variance of the gradient estimators. We have derived score function and reparameterized gradients for each of the divergences in Appendices D and E, following Geffner and Domke (2020b). While a small step size can help to mitigate these challenges to an extent, with increasing dimensions, the variance of the gradients will eventually become large.

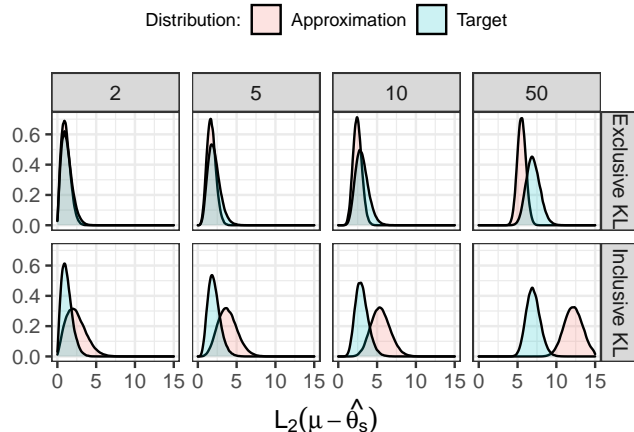


Figure 2: For correlated Gaussian targets in dimensions  $D = 2, 5, 10, 50$ , the marginal distributions of the distance from the mode for samples drawn from the approximation (red) and the target (blue).

### 3.1 Pre-asymptotic reliability case study

To better understand the limitations of different divergences, we investigate their empirical pre-asymptotic behavior. We fit a mean-field Gaussian to a Gaussian with constant 0.5 correlation factor using inclusive KL, exclusive KL,  $\chi^2$ , and  $1/2$ -divergences. We vary the dimensionality  $D$  from 1 to 50. To find the optimal divergence-based approximation, we optimize the closed-form expression for the divergences between two Gaussians. Hence, we can focus on the *best-case scenario* and ignore the complexities and uncertainty due to the stochastic optimization.

Due to space limitations, we focus on representative cases of the approximations from optimising the mode-seeking exclusive KL divergence and the mass-covering inclusive KL divergence. Results for the other divergences are included in the appendix.

**Mode-seeking divergences have more predictable behavior than mass-covering ones.** We begin by comparing how the qualitative behaviors of mode-seeking and mass-covering divergences differ, with Fig. 2 providing a more comprehensive picture of what is illustrated in Fig. 1(c,d).

To cover the posterior’s typical set, the inclusive KL-based approximations must place more mass that is beyond the posterior’s typical set. While this ensures the weights are bounded, when there is a significant mismatch between the geometry of the posterior  $p$  and all  $q \in \mathcal{Q}$  (e.g., when  $D$  is larger), this results in essentially zero overlap between the typical sets of the approximation and the posterior. Therefore, in practice, the weights  $w$  will be very heavy-tailed, giving poor pre-asymptotic behavior. On the other hand, the mode-seeking behavior of the exclusive KL-based approximations leads to the opposite phenomenon: as the mismatch between  $p$  and  $q \in \mathcal{Q}$  increases with  $D$ , the approximations underestimate the distance to the posterior’s typical set.

**The exclusive KL divergence is generally stable across dimensions.** As shown in Fig. 3a (top), the  $\hat{k}$  diagnostic for the optimal exclusive KL variational approximation remains fairly constant as  $D$  increases, particularly for sublinear functions of  $w$ . This

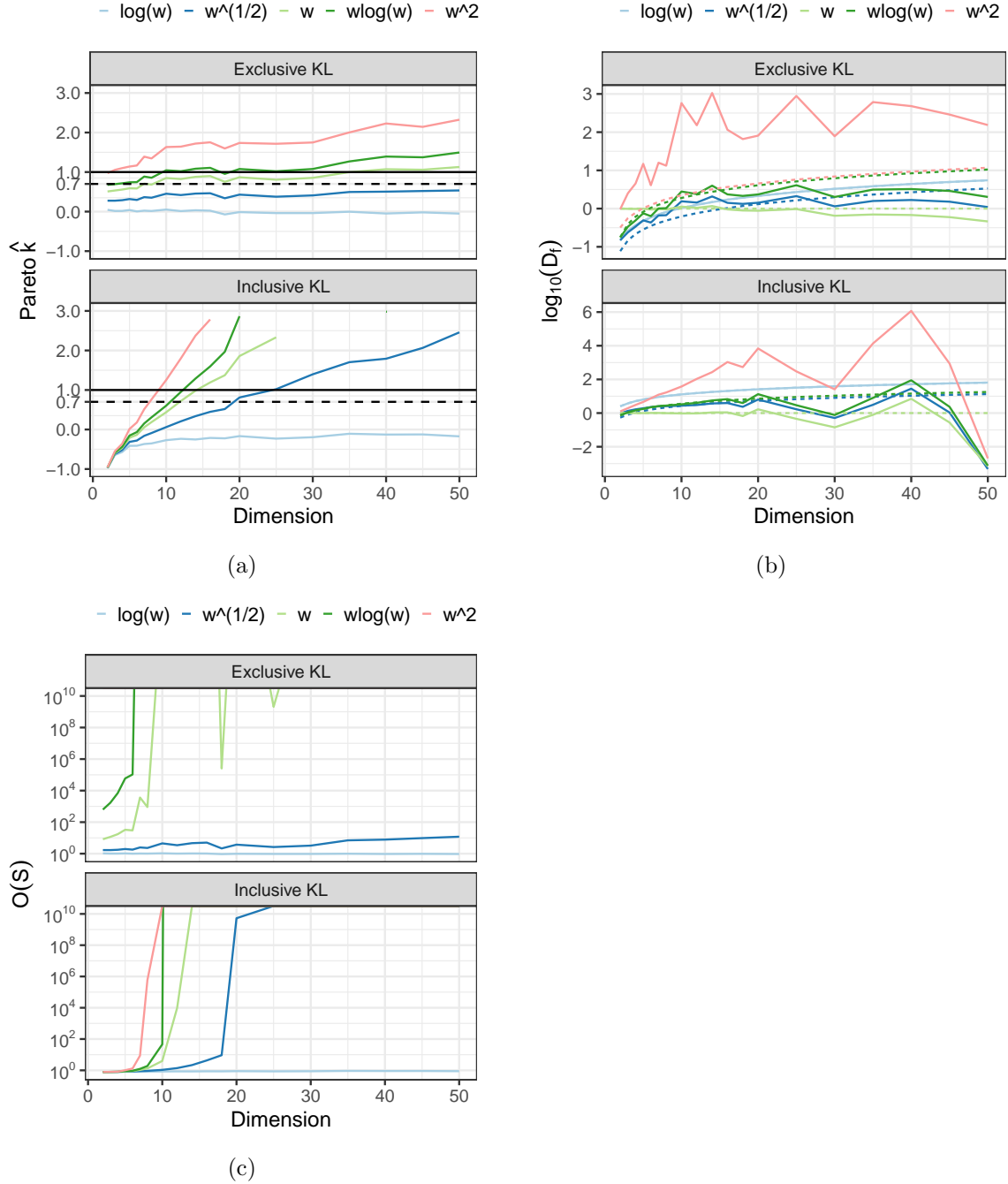


Figure 3: Results for correlated Gaussian targets of dimension  $D = 1, \dots, 50$  using either the exclusive or inclusive KL divergence as the variational objective. **(a)** The  $\hat{k}$  values for the variational approximations. **(b)** The divergence estimate (solid lines) versus analytical (dashed lines) for different  $f(w)$ . **(c)** The estimated minimal sample size required to reliably estimate each  $f(w)$  (using Eq. (6)).

behavior is in agreement with the more predictable behavior of the exclusive KL-based approximation seen in Fig. 2. However, superlinear functions (corresponding to the inclusive KL and  $\chi^2$  divergences) have  $\hat{k} > 0.7$  even when  $D$  is small because of the uncertainty underestimation. Of particular interest is the behavior of  $\hat{k}$  for  $w$ , which indicates whether the variational approximation can be reliably used as a proposal for importance sampling estimates of posterior functionals. For  $w$ ,  $\hat{k} > 0.7$  for relatively easy posteriors ( $D \approx 10$  or greater), but  $\hat{k}$  for  $w$  then remains almost the same as  $D$  continues to increase. Thus, the reliability of exclusive KL-based approximations remains roughly the same across a range of difficulty levels.

**Mass-covering divergences become unstable even for moderately challenging posteriors.** In agreement with Fig. 2, the mass-covering inclusive KL divergence has dramatically different behavior as the dimension increases. As shown in Fig. 3a (bottom), the inclusive KL-based approximations have small  $\hat{k}$  values for all functions of  $w$  up to  $D \approx 5$ , for all but  $w^2$  up to  $D \approx 10$ , and for sublinear functions up to  $D \approx 20$ . However, above  $D \approx 20$  all but  $\log w$  have large  $\hat{k}$  – compare this to the exclusive KL, where  $w^{1/2}$  remains small even up to  $D = 50$ . Thus, while mass-covering divergences seem to perform well on “easy” targets where  $p$  is (nearly) contained in  $\mathcal{Q}$ , their performance deteriorates quickly when there is even a moderate degree of mismatch between  $p$  and  $\mathcal{Q}$ .

**The  $\hat{k}$  diagnostics reflect pre-asymptotic bias.** As seen in Fig. 3b, as the difficulty/dimension increases, the divergence estimates obtained from both the inclusive and exclusive KL-based approximations degrade. In practice, there is a pre-asymptotic bias toward underestimation of the divergences because the distribution of  $w(\theta)$  becomes very heavy-tailed. Notably, the exclusive KL-based approximation bias is consistently small-to-moderate, even when  $D = 50$ , which is in agreement with the  $\hat{k}$  values. On the other hand, the inclusive KL-based approximation bias grows significantly as dimension increases – except for  $\log w$ . Again, this agrees with the  $\hat{k}$  values shown in Fig. 3a and the estimated minimal sample size requirements shown in Fig. 3c.

**Variance of the gradients becomes increasingly large with dimensions.** In Fig. 4 shows that the empirical variance of the gradient of the inclusive KL divergence at the optimal variational approximation grows exponentially in the dimension, while the variance of the exclusive KL gradient grows much more slowly.

In agreement with the earlier  $\hat{k}$  plot and discussion, we should therefore expect optimising the inclusive KL divergence quickly becomes infeasible as the dimension increases since

the gradient variance is too large for stochastic optimization to be effective. In the case of exclusive KL, while the variance is still non-trivial, the behavior is much more robust across dimensionality.

## 4. Experiments

Having established the differing behaviors of mode-seeking and mass-covering divergences for posteriors of varying difficulties, and the value of our pre-asymptotic importance sampling perspective on explaining these differences, we turn to exploring the implications for practical applications. In particular, we must account for the non-Gaussian geometries of many posteriors encountered in practice, the role of stochastic optimization in finding the optimal

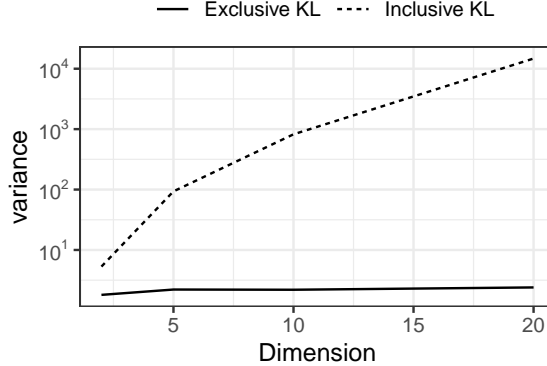


Figure 4: Variance of the gradient for one parameter  $\theta_d$  for increasing dimensions at the end of the optimisation for correlated Gaussian targets of dimension  $D = 1, \dots, 20$  and mean field Gaussian as variational approximation.

variational approximation, and the possibility of using more complex variational families such as normalizing flows.

We compare the accuracy of approximated posterior moments to ground-truth computed either analytically or using the dynamic Hamiltonian Monte Carlo algorithm in Stan (Stan Development Team, 2020).

Specifically, we consider the estimates  $\hat{\mu}$  and  $\hat{\Sigma}$  for, respectively, the posterior mean  $\mu$  and covariance matrix  $\Sigma$ . We also consider the mean and covariance estimates produced by PSIS. Finally, we compute the  $\hat{k}$  diagnostic.

For all posteriors, we fit mean-field Gaussian and Student- $t$  families, a planar flow with 6 layers and an NVP flow with 6 stacked neural networks with 2 hidden layers of 10 neurons each for both the translation and scaling operations with a standard Gaussian prior on the latent factor. We use **Stan** (Stan Development Team, 2020) for model construction. For stochastic optimization we use RMSProp with initial step size of  $10^{-3}$  run for either  $T_{\max}$  iterations or until convergence was detected using a modified version of the algorithm by Dhaka et al. (2020). For the exclusive KL we use 10 draws for gradient estimation per iteration, while for other divergences we use 200 draws, and a warm start at the solution of the exclusive KL. In practice, we found the optimisation for  $\chi^2$  divergence extremely challenging, with the solution failing to converge even for moderate dimensions  $D > 10$ . Therefore, we only include results for the KL divergences and the adaptive  $f$ -divergence.

#### 4.1 Heavy-tailed posteriors

To confirm our findings from the previous section on a more realistic example and explore the behavior of the adaptive  $f$ -divergence, we begin by fitting the toy robust regression model previously used by Huggins et al. (2020). The assumed model is

$$\beta_d \sim \mathcal{N}(0, 10), \quad y_n | x_n, \beta \sim t_{10}(\beta^\top x_n, 1),$$

where  $y_n \in \mathbb{R}, x_n \in \mathbb{R}^D$  are the target and predictors respectively,  $\beta$  denotes the unknown coefficients, and  $D$  is varied from 2 to 50. We generated data from the same model with covariates generated from a zero-mean Gaussian with constant correlation of 0.4. The

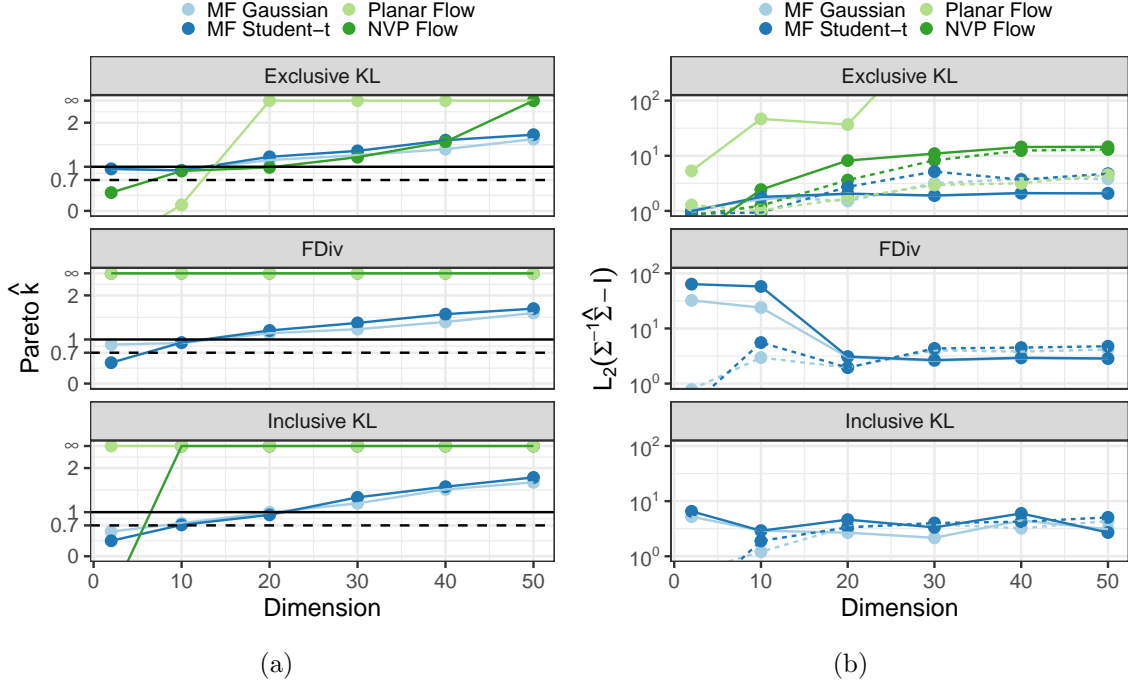


Figure 5: Results for increasing dimensions of the robust regression model. **(a)** Pareto  $\hat{k}$  values for BBVI approximations. **(b)** Relative error of covariance estimates for BBVI (solid lines) and after PSIS correction (dashed lines).

Student- $t$  leads to the posterior having heavy tails, making it a more challenging target. We use  $T_{\max} = 10,000$ .

**Mode-seeking divergences are easier to optimize.** We summarise the results in Fig. 5.

In general, the exclusive KL performs better than the inclusive KL, particularly when using normalizing flows, as seen in the smaller  $\hat{k}$  and errors. The better performance on normalizing flows corroborates the relative ease of the exclusive KL stochastic optimization problem compared to using inclusive KL or adaptive  $f$ -divergence.

**Adaptive  $f$ -divergence interpolates exclusive and inclusive KL divergence, but is difficult to optimize.** As can be seen visually and via the  $\hat{k}$  values in Fig. 6, the adaptive  $f$ -divergence behaves somewhere between the two KL divergences – as it was designed to (Wang et al., 2018). For higher-dimensional posteriors, we expect it to behave more like the exclusive KL. But, due to its reliance on the importance weights, is less stable – as confirmed by Fig. 5.

**Normalizing flows can be effective but are challenging to optimize.** Fig. 5 also show that normalizing flows can be quite effective when used with exclusive KL to ensure stable optimization. However, as can be seen in Fig. 6, when using out-of-the-box optimization with no problem-specific tuning (as we have done for a fair comparison), the NF posterior approximations will have some pathological features – even in low dimensions.



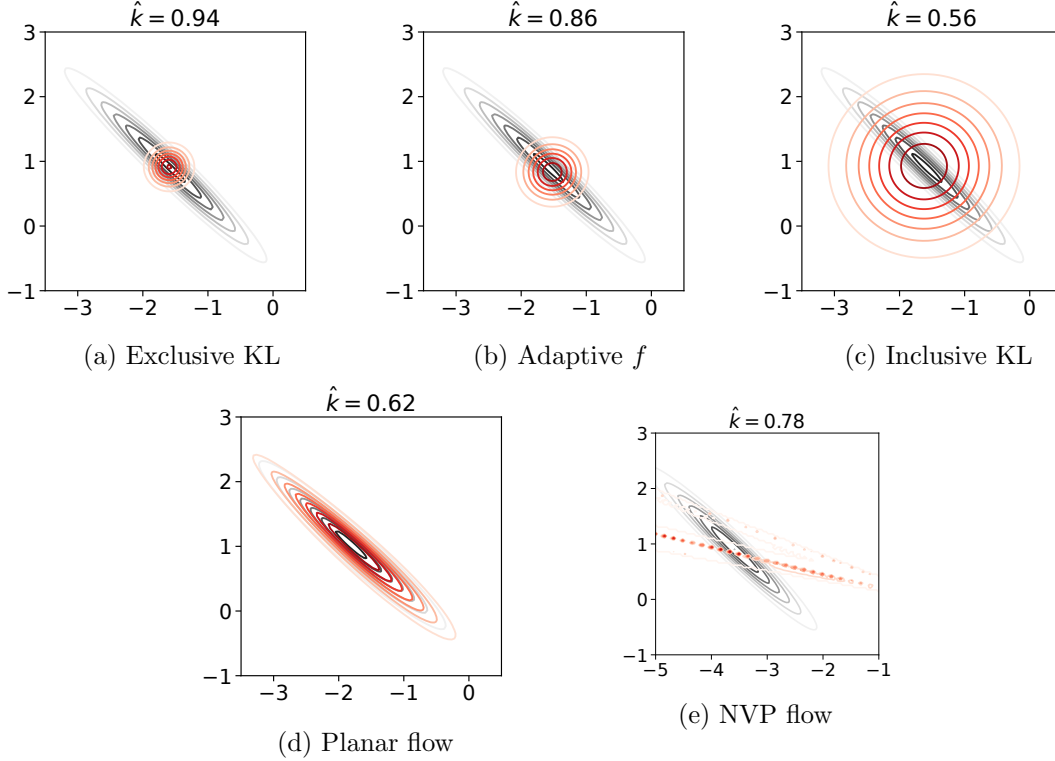


Figure 6: Variational approximations (red) for robust regression posterior (black) with  $D = 2$ . (a–c) Uses mean-field Gaussian family. (d,e) Uses exclusive KL divergence.

## 4.2 Realistic models and datasets

To better understand how divergences and approximating families compare across a diverse range of realistic posteriors, we consider models and datasets taken from `posteriordb`<sup>\*</sup>. We use  $T_{\max} = 15,000$ .

**Exclusive KL remains the most reliable for realistic posteriors.** In Section 4.1, we see the same patterns: exclusive KL is superior for higher-dimensional posteriors (e.g.,  $D > 10$ ) or when combined with normalizing flows, while inclusive KL is better for lower-dimensional posteriors. Even when using exclusive KL, the optimization challenges with normalizing flows are apparent in the large  $\hat{k}$  values for the higher-dimensional posteriors. The adaptive  $f$ -divergence did not clearly outperform either KL divergence.

**Importance sampling can substantially improve accuracy.** Focusing on exclusive KL, Fig. 7b shows that across all scenarios, using importance sampling (specifically, PSIS) either improved or had no effect on the approximation accuracy. In some cases, PSIS dramatically improved the accuracy of the normalizing flows.

**Reparameterization is an important tool for improving accuracy.** The 8-schools model has a low dimensional  $D = 10$  but funnel-shaped posterior that makes inference challenging for variational approximations (Huggins et al., 2020; Yao et al., 2018). As has been noted previously in the literature, and is clear from Section 4.1 and Fig. 7b,

<sup>\*</sup>. <https://github.com/stan-dev/posteriordb>

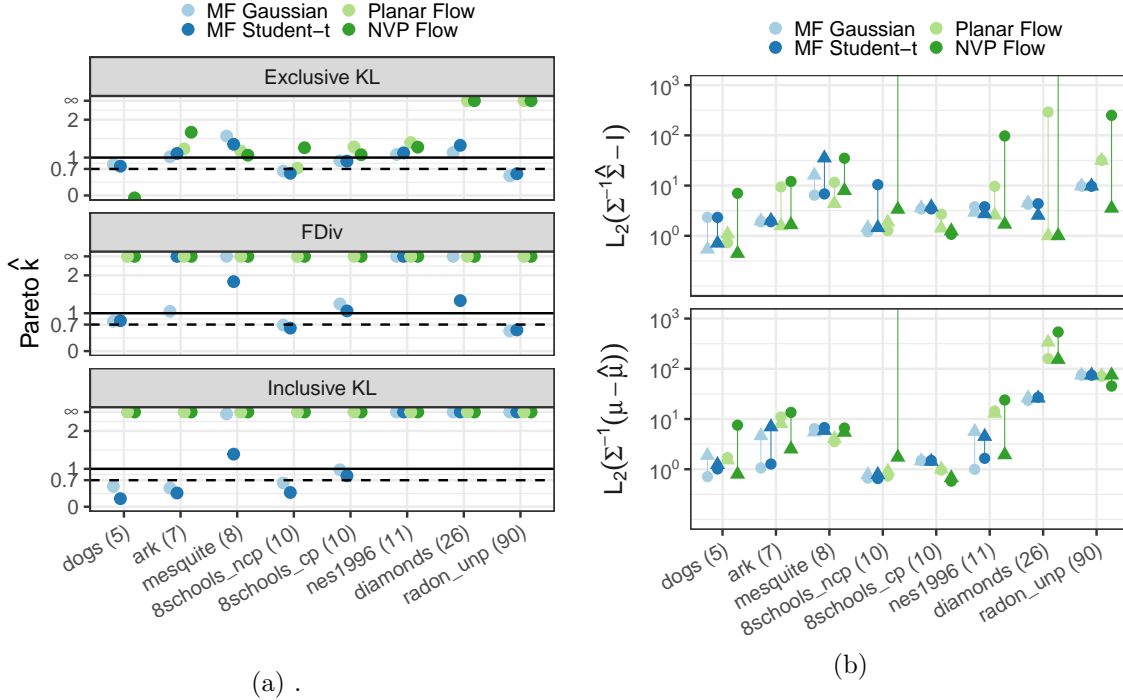


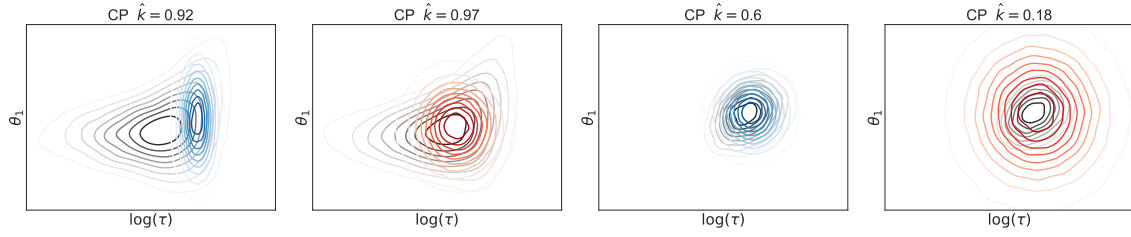
Figure 7: Results for `posterior`db experiments. (a) Pareto  $\hat{k}$  values for BBVI approximations. (b) Relative error of mean and covariance estimates for BBVI (circles) and after PSIS correction (triangles).

reparameterizing the model so the posterior better matches the variational family can be an effective way to improve the variational approximation. See visual illustration in Section 4.2.

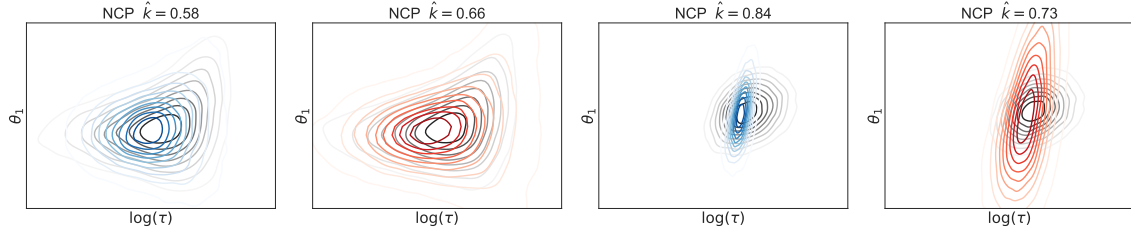
## 5. Discussion

Our conceptual framework based on the pre-asymptotic behavior of the density ratios / importance weights  $w$  along with our comprehensive experiments lead to a number of important takeaways for practitioners looking to obtain reasonably accurate posterior approximations using black-box variational inference:

- The instability of mass-covering divergences like inclusive KL and  $\chi^2$  means that, given currently available methodology, users are better off using the exclusive KL divergence except for easy low-dimensional posteriors. The reliance of the adaptive  $f$ -divergence on importance weights leads to similar instability.
- Importance sampling appears to almost always be beneficial for improving accuracy, even when the  $\hat{k}$  diagnostic is large. However, a large  $\hat{k}$  does suggest the user should not expect even the PSIS-corrected estimates to be particularly accurate.
- Using normalizing flows – particularly NVP flows – together with exclusive KL and PSIS provides the best and most consistent performance across posteriors of varying dimensionality and difficulty. We therefore suggest this combination as a good default choice.



(a) results with centered parameterisation(CP) on standard eight schools and eight schools with more informative data.



(b) results with non-centered parameterisation(NCP) on standard eight schools and eight schools with more informative data.

Figure 8: Plots for the approximate posteriors obtained by optimizing exclusive KL(blue) and inclusive KL(red).

Our results suggest an important direction for future work is improving the stability of optimization with normalizing flows, which still tend to have some pathological behaviors unless they are very carefully tuned since such tuning significantly detracts from the benefits of using BBVI.

## 6. Acknowledgments

We acknowledge the computational resources provided by the Aalto Science-IT project and support by the Academy of Finland Flagship programme: Finnish Center for Artificial Intelligence, FCAI.

## REFERENCES

- Abhinav Agrawal, Daniel R. Sheldon, and Justin Domke. Advances in black-box VI: normalizing flows, importance weighting, and optimization. In *Advances in Neural Information Processing Systems 33: Annual Conference on Neural Information Processing Systems 2020, NeurIPS 2020, December 6-12, 2020, virtual*, 2020.
- Robert Bamler, Cheng Zhang, Manfred Opper, and Stephan Mandt. Perturbative black box variational inference. In *Advances in Neural Information Processing Systems*, volume 30, pages 5079–5088, 2017.

C. M. Bishop. *Pattern Recognition and Machine Learning*. Springer, 2006.

- D. M. Blei, Alp Kucukelbir, and Jon D McAuliffe. Variational Inference: A Review for Statisticians. *Journal of the American Statistical Association*, 112(518):859–877, 2017.
- Jörg Bornschein and Yoshua Bengio. Reweighted wake-sleep. In *3rd International Conference on Learning Representations, ICLR 2015, San Diego, CA, USA, May 7-9, 2015, Conference Track Proceedings*, 2015.
- Sourav Chatterjee and Persi Diaconis. The sample size required in importance sampling. *Ann. Appl. Probab.*, 28(2):1099–1135, 2018. doi: 10.1214/17-AAP1326.
- Louis H Y Chen and Qi-Man Shao. Normal approximation under local dependence. *The Annals of Probability*, 32(3):1985–2028, 2004.
- Akash Kumar Dhaka, Alejandro Catalina, Michael R Andersen, Måns Magnusson, Jonathan Huggins, and Aki Vehtari. Robust, accurate stochastic optimization for variational inference. In *Advances in Neural Information Processing Systems*, volume 33, pages 10961–10973, 2020.
- Adji Bousso Dieng, Dustin Tran, Rajesh Ranganath, John Paisley, and David Blei. Variational inference via  $\chi$  upper bound minimization. In *Advances in Neural Information Processing Systems 30*, pages 2732–2741. 2017.
- Laurent Dinh, Jascha Sohl-Dickstein, and Samy Bengio. Density estimation using real nvp. In *International Conference on Learning Representations*, 2017.
- John Duchi, Elad Hazan, and Yoram Singer. Adaptive Subgradient Methods for Online Learning and Stochastic Optimization. *Journal of Machine Learning Research*, 12:2121–2159, 2011.
- Ilenia Epifani, Steven N MacEachern, and Mario Peruggia. Case-deletion importance sampling estimators: Central limit theorems and related results. *Electronic Journal of Statistics*, 2:774–806, 2008.
- Tomas Geffner and Justin Domke. On the difficulty of unbiased alpha divergence minimization, 2020a.
- Tomas Geffner and Justin Domke. Empirical evaluation of biased methods for alpha divergence minimization. In *Symposium on Advances in Approximate Bayesian Inference, AABI 2020*, 2020b.
- John Geweke. Bayesian inference in econometric models using Monte Carlo integration. *Econometrica*, 57(6):1317–1339, 1989. ISSN 00129682, 14680262.
- Shixiang (Shane) Gu, Zoubin Ghahramani, and Richard E Turner. Neural adaptive sequential Monte Carlo. In *Advances in Neural Information Processing Systems*, volume 28, pages 2629–2637, 2015.
- Jose Hernandez-Lobato, Yingzhen Li, Mark Rowland, Thang Bui, Daniel Hernandez-Lobato, and Richard Turner. Black-box alpha divergence minimization. In *Proceedings of The 33rd International Conference on Machine Learning*, volume 48, pages 1511–1520. PMLR, 2016.

- G. E. Hinton and Tijmen Tieleman. Lecture 6.5 – Rmsprop: Divide the gradient by a running average of its recent magnitude. In *Coursera: Neural networks for machine learning*, 2012.
- Jonathan H Huggins, Mikolaj Kasprzak, Trevor Campbell, and T. Broderick. Validated Variational Inference via Practical Posterior Error Bounds. In *AISTATS*, 2020.
- Alp Kucukelbir, Rajesh Ranganath, Andrew Gelman, and D. M. Blei. Automatic Variational Inference in Stan. In *Advances in Neural Information Processing Systems*, Advances in Neural Information Processing Systems, 2015.
- Yingzhen Li and Richard E Turner. Rényi divergence variational inference. In *Advances in Neural Information Processing Systems*, volume 29, pages 1073–1081, 2016.
- Wu Lin, Mohammad Emtiyaz Khan, and Mark Schmidt. Fast and Simple Natural-Gradient Variational Inference with Mixture of Exponential-family Approximations. In *International Conference on Machine Learning*, 2019.
- David J. C. MacKay. *Information Theory, Inference and Learning Algorithms*. Cambridge University Press, 2003.
- Andrew C. Miller, Nicholas J. Foti, and Ryan P. Adams. Variational boosting: Iteratively refining posterior approximations. In *Proceedings of the 34th International Conference on Machine Learning*, volume 70 of *Proceedings of Machine Learning Research*, pages 2420–2429. PMLR, 2017.
- Shakir Mohamed, Mihaela Rosca, Michael Figurnov, and Andriy Mnih. Monte Carlo gradient estimation in machine learning. *arXiv preprint arXiv:1906.10652*, 2019.
- Christian A. Naesseth, Fredrik Lindsten, and David M. Blei. Markovian score climbing: Variational inference with  $\text{kl}(p||q)$ . *CoRR*, abs/2003.10374, 2020.
- Victor M H Ong, David J Nott, and Michael S Smith. Gaussian Variational Approximation With a Factor Covariance Structure. *Journal of Computational and Graphical Statistics*, 27(3):465–478, 2018. doi: 10.1080/10618600.2017.1390472.
- Danilo Rezende and Shakir Mohamed. Variational inference with normalizing flows. In *Proceedings of the 32nd International Conference on Machine Learning*, volume 37 of *Proceedings of Machine Learning Research*, pages 1530–1538. PMLR, 2015.
- Geoffrey Roeder, Yuhuai Wu, and D Duvenaud. Sticking the Landing: Simple, Lower-Variance Gradient Estimators for Variational Inference. In *Neural Information Processing Systems*, 2018.
- Stan Development Team. Stan modeling language users guide and reference manual. 2.26, 2020. URL <https://mc-stan.org>.
- Aki Vehtari, Daniel Simpson, Andrew Gelman, Yao Yuling, and Jonah Gabry. Pareto smoothed importance sampling. *arXiv preprint arXiv:1507.02646*, 2019.

- Neng Wan, Dapeng Li, and Naira Hovakimyan. f-Divergence Variational Inference. In *Advances in Neural Information Processing Systems*, 2020.
- Dilin Wang, Hao Liu, and Qiang Liu. Variational inference with tail-adaptive f-divergence. In *Advances in Neural Information Processing Systems*, volume 31, pages 5737–5747, 2018.
- Ming Xu, Matias Quiroz, Robert Kohn, and Scott A. Sisson. Variance reduction properties of the reparameterization trick. In *Proceedings of Machine Learning Research*, volume 89 of *Proceedings of Machine Learning Research*, pages 2711–2720. PMLR, 2019.
- Yuling Yao, Aki Vehtari, Daniel Simpson, and Andrew Gelman. Yes, but did it work?: Evaluating variational inference. In *Proceedings of the 35th International Conference on Machine Learning*, volume 80 of *Proceedings of Machine Learning Research*, pages 5581–5590. PMLR, 2018.

Table A.1: Datasets from PosteriorDB.

Name	Dimensions
Dogs	5
Ark	7
Mesquite	8
Eight schools non centered	10
Eight schools centered	10
NES1996	11
Diamonds	26
Radon unpooled	90

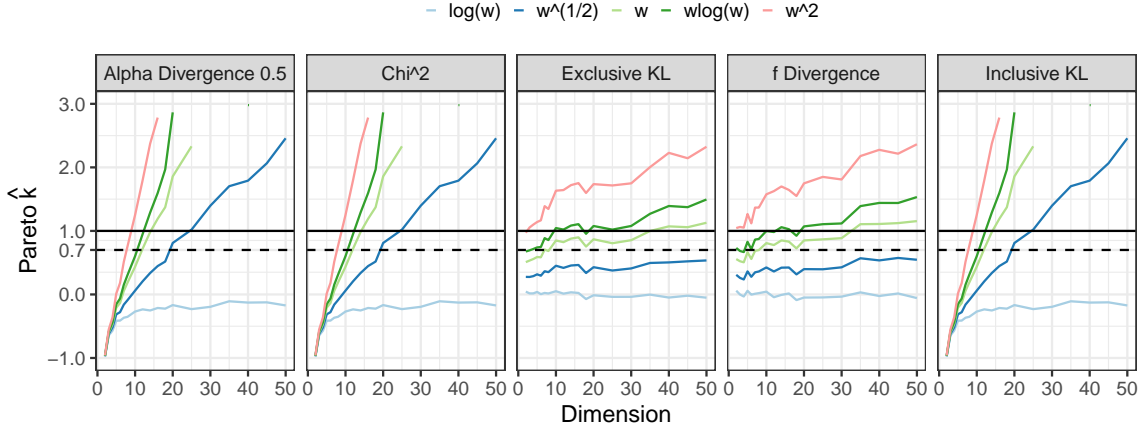


Figure B.1: Pareto  $\hat{k}$  estimated for different objectives and divergences estimation for a 0.5 correlated Gaussian target and mean field Gaussian approximation and increasing dimensionality.

## Appendix A. PosteriorDB datasets

In Table A.1 we show the dimensionality of the datasets we use for our real experiments.

## Appendix B. Additional results for the pre-asymptotic reliability case study

In Fig. B.1 and Fig. B.2 we show additional results for the pre-asymptotic reliability case study for different objectives and mean field Gaussian approximation. The results from optimising  $\chi^2$ ,  $1/2$ -divergence and tail adaptive  $f$ -divergence follow similar trends as those resulting from optimising exclusive and inclusive KL. Approximations obtained by optimising  $\chi^2$  and  $1/2$ -divergence are more unstable and end up diverging in similar ways as inclusive KL even for moderately low dimensional problems. We use a warm start procedure for

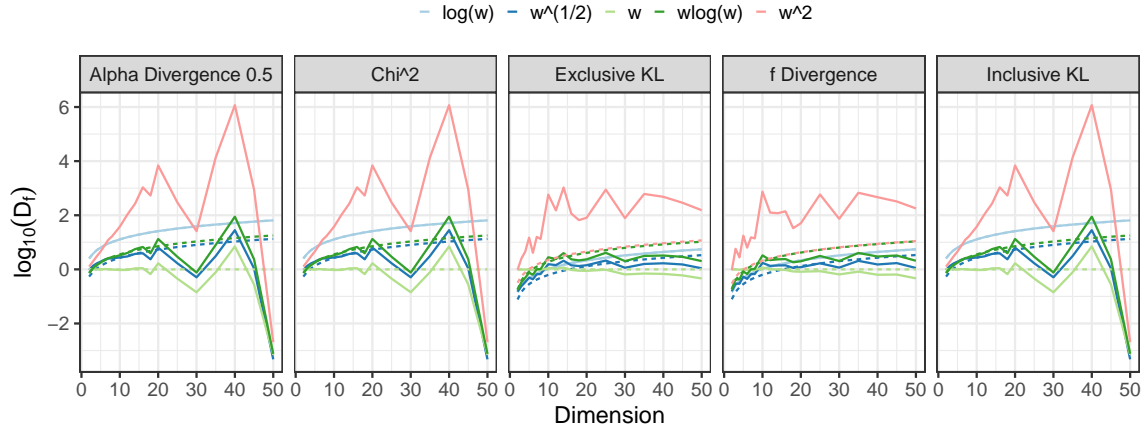


Figure B.2: Divergences estimates for different objectives for a 0.5 correlated Gaussian target and mean field Gaussian approximation and increasing dimensionality.

$\chi^2$ ,  $1/2$ -divergence and inclusive KL, starting at the solution of exclusive KL for a given problem. On the other hand, optimising tail adaptive  $f$ -divergence seems to be more robust and behave similarly to exclusive KL even in higher dimensions.

## Appendix C. Additional experiments

**Isolating the effect of variational family.** In this section, we perform a systematic comparison of inclusive-KL and exclusive KL divergences using mean-field Gaussian and mean-field Student- $t$  approximation families for varying amount of correlation and dimensionality of the underlying parameter space. The dimension size is varied from 2 to 100. For Gaussian target with Gaussian approximation, we used BFGS as the optimiser removing any error due to stochastic optimisation. The plots in Fig. C.1 show how  $\hat{k}$  behaves with increasing dimension and increasing correlation in posterior for a mean field Gaussian approximation and optimising objectives for exclusive KL and inclusive-KL divergences respectively. We also plot a similar plot for planar-flow when optimising exclusive KL divergence. The plots indicate even when the approximation is heavy tailed and divergence measure is *mass covering*, the final variational mean field approximation becomes unreliable. The dimension at which this happens depends on the posterior geometry (correlation in this case). Since the target is Gaussian, when the approximation is Gaussian family, we can estimate exclusive and inclusive KL analytically at the optimisation end points for each of the divergences, for the other approximations, Student's  $t$  and planar flow, we estimate these quantities by MC.

Extensive experiments and results are shown in Fig. C.2, Fig. C.3, Fig. C.4 and Fig. C.5



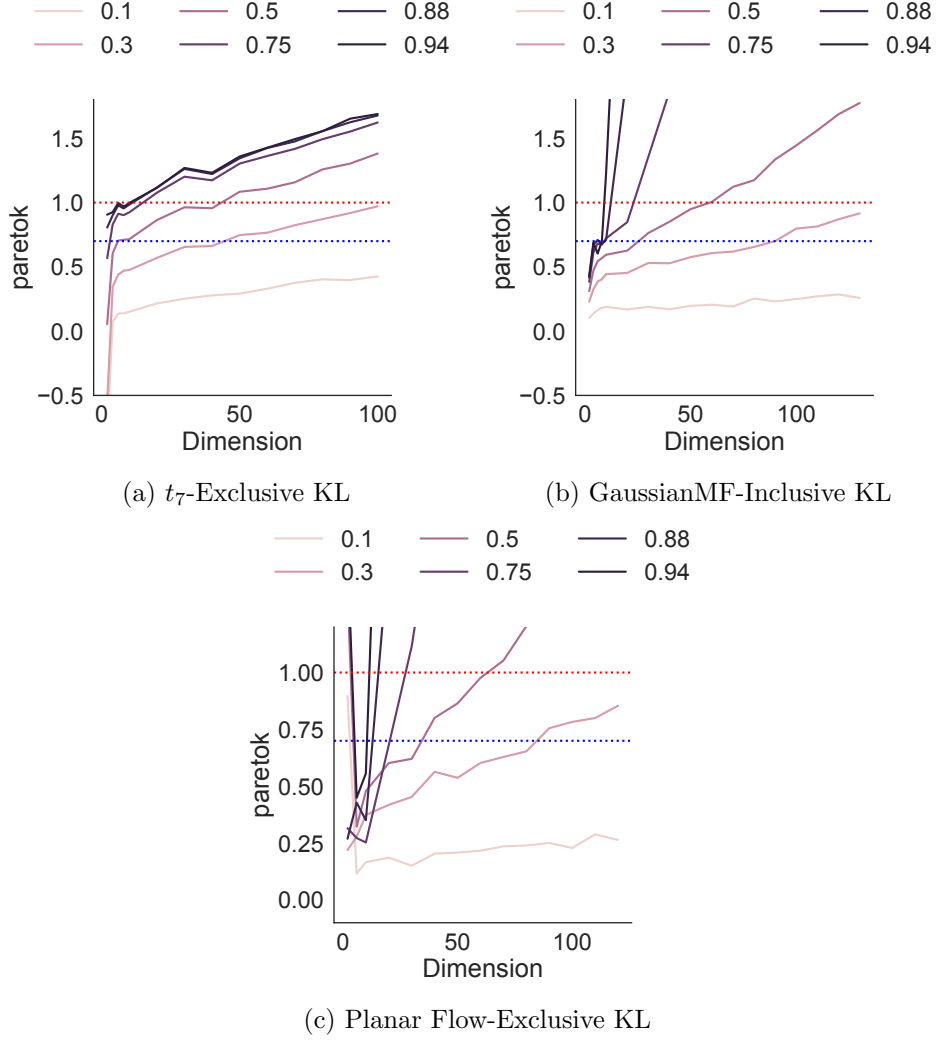


Figure C.1: Plots of  $\hat{k}$  with Exclusive KL divergence minimisation, Inclusive KL divergence minimisation with mean-field Student- $t$  density and with Planar Flows for increasing correlation and dimensions.

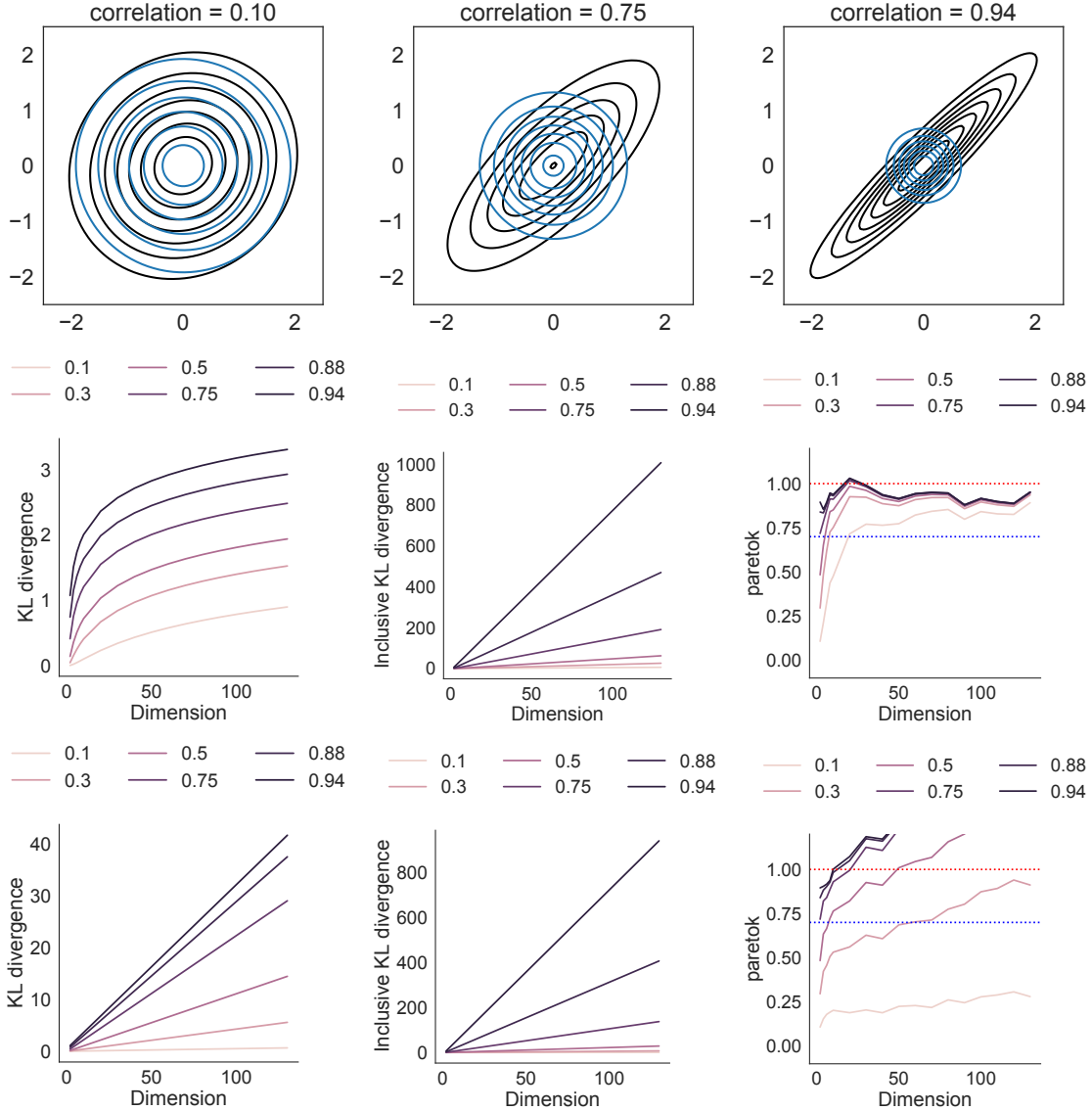


Figure C.2: Gaussian mean field solution for exclusive KL divergence. The top row shows solutions obtained after minimizing the exclusive KL divergence where the target is a correlated Gaussian density with varying amount of correlations, and the approximation is a mean field approximation. The second row shows plots from the left to the right: the exclusive KL divergence, the inclusive KL divergence and the Pareto  $k$  statistic computed at the solution returned by BFGS optimisation for increasing dimensions and different amount of correlations when the target has a uniform covariance structure, the bottom row shows the corresponding plots for banded covariance target.

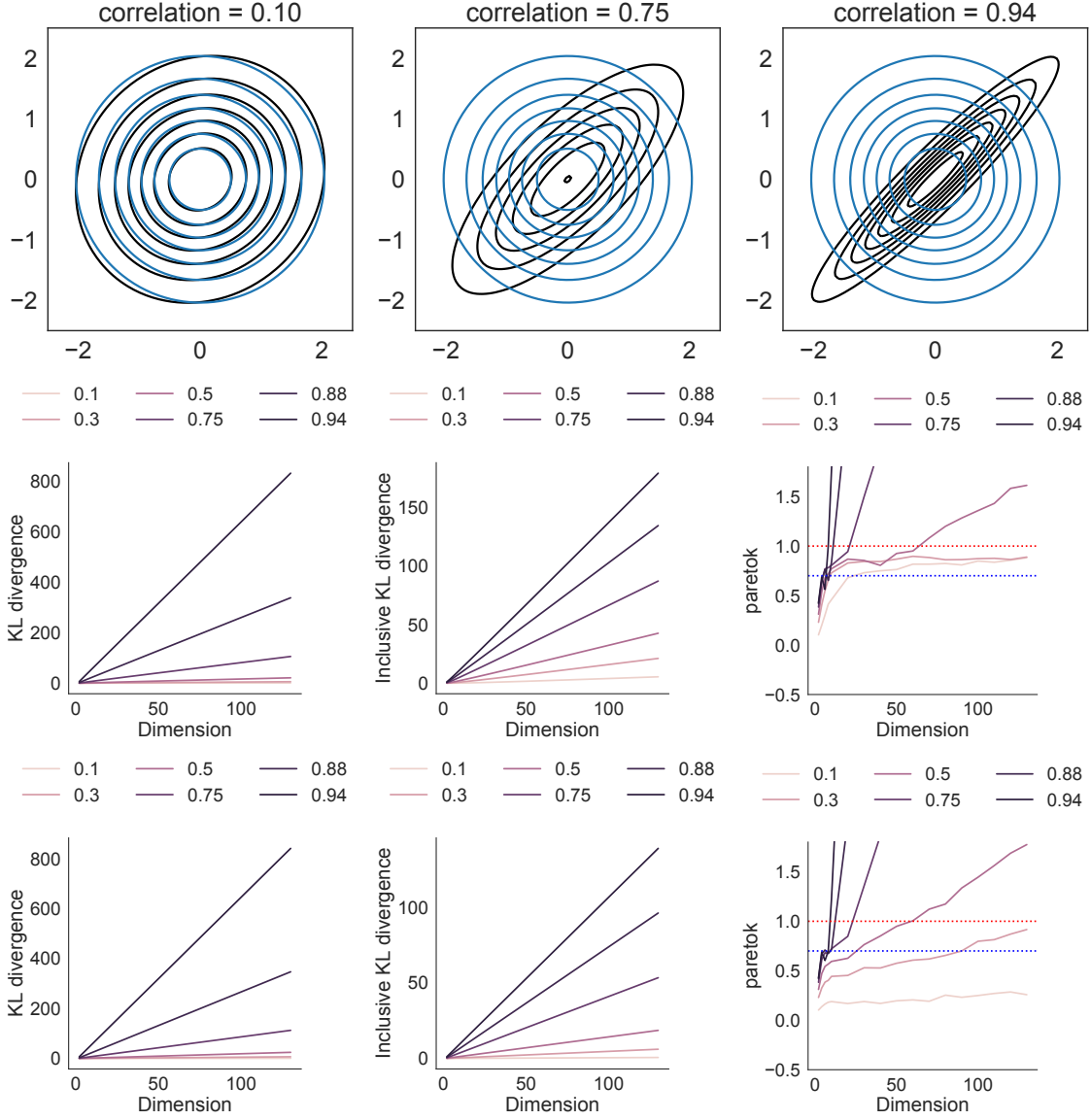


Figure C.3: Gaussian mean field solution for inclusive KL divergence. The top row shows solutions obtained after minimizing the exclusive KL divergence where the target is a correlated Gaussian density with varying amount of correlations, and the approximation is a mean field approximation. The second row shows plots from the left to the right: the exclusive KL divergence, the inclusive KL divergence and the Pareto  $k$  statistic computed at the solution returned by BFGS optimisation for increasing dimensions and different amount of correlations when the target has a uniform covariance structure, the bottom row shows the same corresponding plots for banded covariance target.

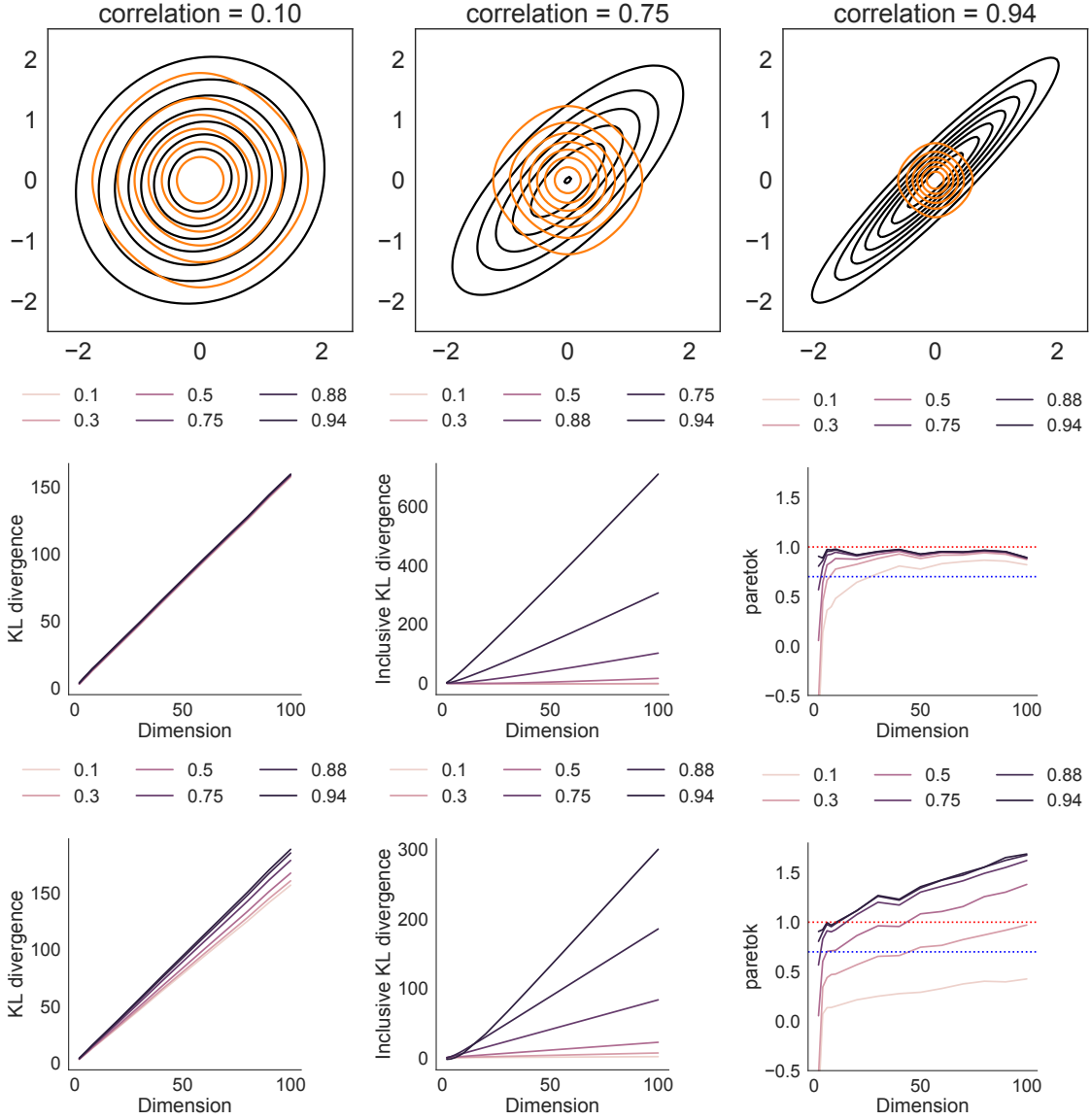


Figure C.4: Solution for exclusive KL divergence where the family of approximation is a product of t-densities. The top row shows solutions obtained after minimizing the exclusive KL divergence where the target is a correlated Gaussian density with varying amount of correlations, and the approximation is a mean field approximation. The second row shows plots from the left to the right: the exclusive KL divergence, the inclusive KL divergence and the Pareto  $k$  statistic computed at the solution returned by stochastic optimisation for increasing dimensions and different amount of correlations when the target has a uniform covariance structure, the bottom row shows the same corresponding plots for banded covariance target.

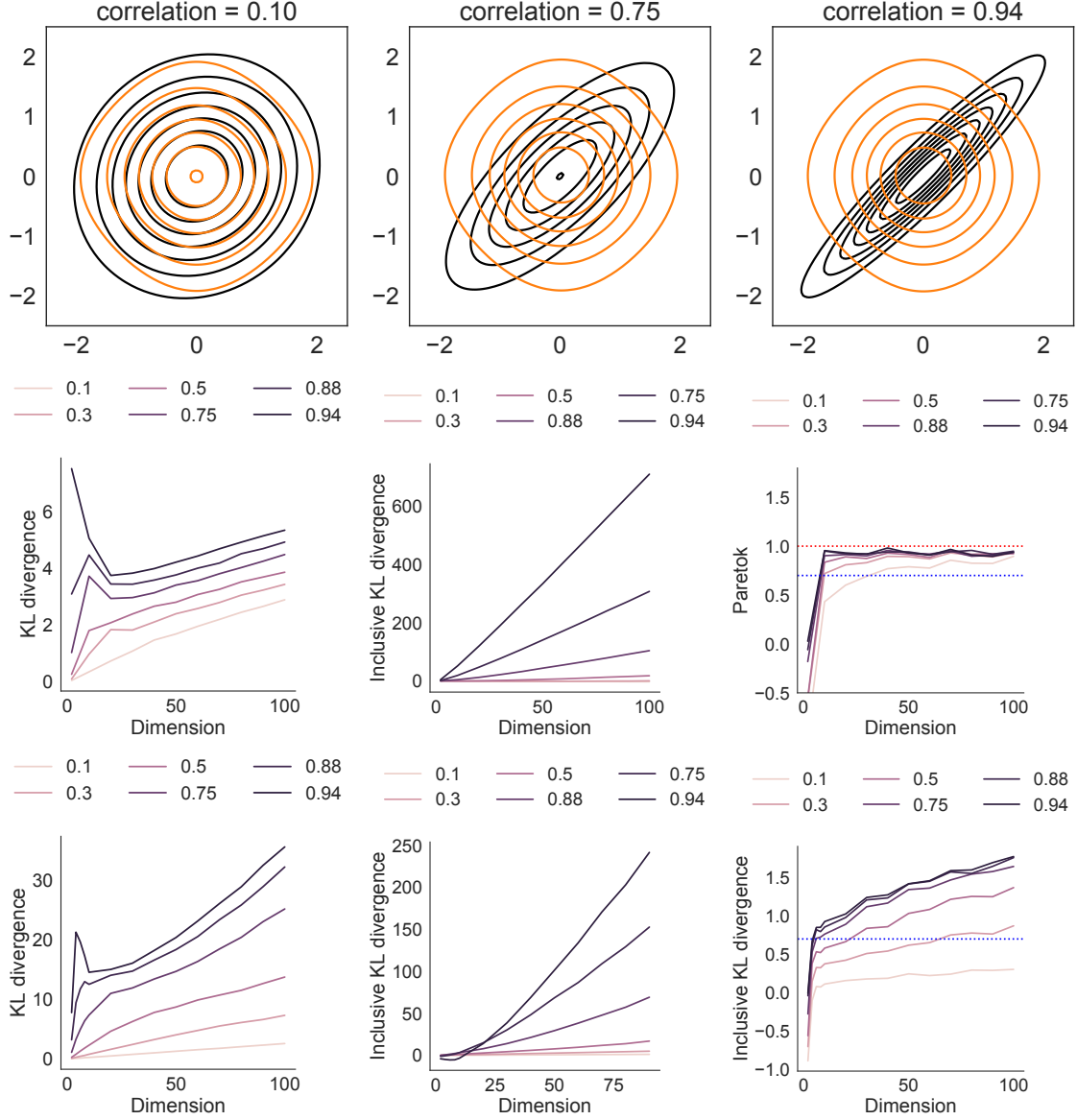


Figure C.5: Solution for inclusive KL divergence where the family of approximation is a product of t-densities. The top row shows solutions obtained after minimizing the inclusive KL divergence where the target is a correlated Gaussian density with varying amount of correlations, and the approximation is a mean field approximation. The second row shows plots from the left to the right: the exclusive KL divergence, the inclusive KL divergence and the Pareto  $k$  statistic computed at the solution returned by stochastic optimisation for increasing dimensions and different amount of correlations when the target has a uniform covariance structure, the bottom row shows the same corresponding plots for banded covariance target.

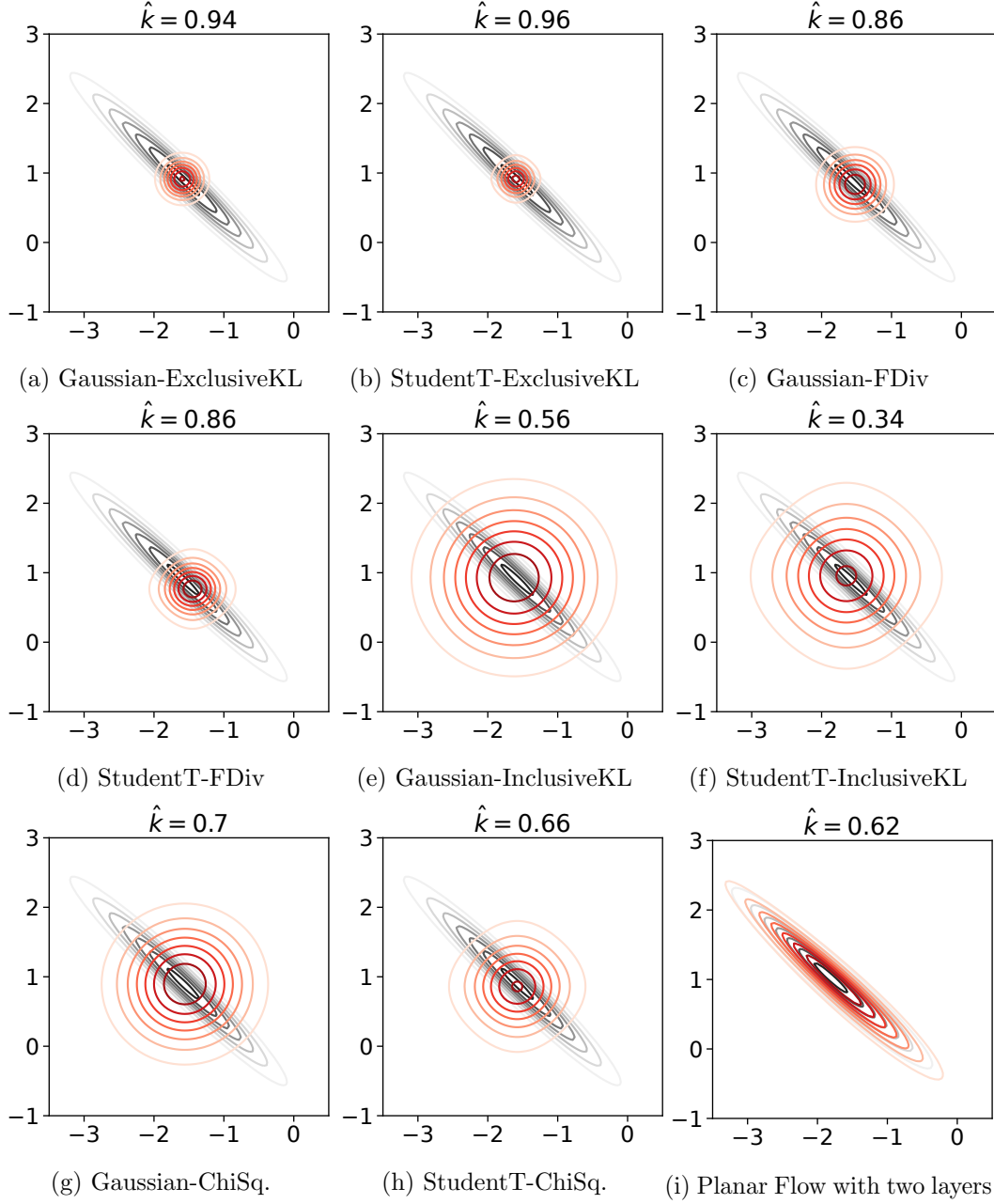


Figure C.6: Approximation for Robust Regression with different divergences and approximation families in 2 dimensions. This shows the properties of divergences and approximations in low dimensions.

## Appendix D. Score function additional discussion

The score function gradient for exclusive KL is given as:

$$\begin{aligned}\nabla_\lambda L(\lambda) &= \nabla_\lambda E_q[\log p(Y, \theta) - \log q(\theta)] \\ &= E_{q_\lambda(\theta)}[\log p(Y, \theta) - \log q(\theta)] \cdot \nabla_\lambda \log q(\theta) \\ &\approx \frac{1}{S} \sum_{s=1}^S [\log w_s \nabla_\lambda \log q_\lambda(\theta_s)],\end{aligned}$$

where we have defined  $w_s = w(\theta_s)$ . If the entropy of the approximate distribution is known analytically, we get another unbiased gradient estimator, where we use the MC samples only to estimate the first part, removing any direct dependence of gradient wrt  $w(\theta_s)$

$$\nabla_\lambda \hat{L}(\lambda) = \frac{1}{S} \sum_{s=1}^S [\log p(Y, \theta_s) \nabla_\lambda \log q_\lambda(\theta_s)] + \nabla_\lambda H_q[q_\lambda(\theta_s)].$$

For inclusive KL divergence, the score function gradient is given as:

$$\nabla_\lambda L(\lambda) = - \sum_{s=1}^S \frac{w_s}{\sum_{s=1}^S w_s} \nabla_\lambda \log q_\lambda(\theta_s). \quad (\text{D.1})$$

where the gradient has been estimated by self-normalised importance sampling (Gu et al., 2015; Bornschein and Bengio, 2015; Li and Turner, 2016).

Similarly, the score gradient for  $\chi^2$  and  $\alpha$  divergences is given as

$$\nabla_\lambda L(\lambda) = \frac{-1}{S} \sum_{s=1}^S [w_s^{\text{score}}]^\alpha \nabla_\lambda \log q(\theta_s; \lambda),$$

where  $\alpha \geq 2$

It is apparent immediately that the gradients will have even higher variance than observed in the case of importance sampling. Importance sampling is known not to work well in higher dimensions, since the variance of the importance weights is likely to become very large or infinite.

The variance of the score gradients for the divergences discussed above as a function of density ratios is given below:

$$\begin{aligned}V_q(G_{\text{CUBO}}^{\text{score}}) &= O(w^4), \\ V_q(G_{\text{Inclusive KL}}^{\text{score}}) &= O(w^2), \\ V_q(G_{\text{InclusiveKL}}^{\text{score}}) &= O(\log(w)^2).\end{aligned}$$

The higher the power on density ratio, the faster the variance of the gradients will grow. This means the density ratio should have finite higher moments for CLT to apply as discussed in Section 2.

## Appendix E. Reparameterised gradients additional discussion

For exclusive KL, the reparameterised gradient becomes

$$\nabla_{\lambda} \mathbb{E}_q[\log j(\theta)] = \mathbb{E}_p[\nabla_{\lambda} T_{\lambda}(\epsilon) \nabla_{\theta} \log j(\theta)]. \quad (\text{E.1})$$

In the case of  $\chi^2$  divergence, the reparameterised gradient is

$$\nabla_{\lambda} \hat{\mathbf{L}}(\lambda) = \frac{2}{S} \sum_{s=1}^S \left( \frac{j(T_{\lambda}(\epsilon_s))}{q(T_{\lambda}(\epsilon_s))} \right)^2 \nabla_{\lambda} \log \left( \frac{j(T_{\lambda}(\epsilon_s))}{q(T_{\lambda}(\epsilon_s))} \right),$$

which can be expressed in terms of density ratios as follows:

$$\nabla_{\lambda} \hat{\mathbf{L}}(\lambda) = \frac{2}{S} \sum_{s=1}^S (w_s^{\text{RP}})^2 \nabla_{\lambda} \log (w_s^{\text{RP}}), \quad (\text{E.2})$$

where the new weights  $w^{\text{RP}}$  denote that they have been evaluated on samples obtained using the reparameterisation trick. In this case, the dependence of the gradient is not straightforward and also depends on the the product of the density ratio squared and its corresponding gradient.

## Appendix F. Covariance Structures

In this work, we use two types of covariance matrices, uniform matrices denoted by  $U$ :  $K_{ij} = 1.[i = j] + \rho[i \neq j]$  and the banded structure, denoted by  $B$ :  $K_{ij} = 1.[i = j] + \rho^{|i-j|}[i \neq j]$

## Appendix G. Gradient Variances for Score function gradient and RP gradient

We want to see how the variance of the gradients for different divergence objectives varies by extending the analysis from Xu et al. (2019) Let us consider the log joint density cost function i.e  $j(\theta) = \log p(Y, \theta) = \theta^2$  and  $q(\theta) = \mathcal{N}(\mu, 1)$

Then for exclusive KL divergence, the RP gradient estimator is:

$$G^{\text{RP}} = \nabla_{\lambda} \mathbb{E}_q[j(\theta)] \quad (\text{G.1})$$

$$G^{\text{RP}} = \mathbb{E}_{\epsilon}[\Delta_{\mu}^{\text{RP}}] = \mathbb{E}_{\epsilon}[\nabla_{\mu} T(\epsilon; \lambda) \nabla_{\theta} j(\theta)] \quad (\text{G.2})$$

$$\Delta_{\mu}^{\text{RP}}(\text{KL}(q||p)) = 1.(2\theta) = 2(\mu + \epsilon) \quad (\text{G.3})$$

$$\mathbb{V}(\Delta_{\mu}^{\text{RP}}(\epsilon; \lambda)(\mu))(\text{KL}(q||p)) = 4 \quad (\text{G.4})$$

Since the gradient wrt the location parameter is a r.v, we can compute the variance under the standard distribution  $N(0, 1)$ . Similarly we can derive the variance of the score function gradient

$$G^{\text{score}}(\lambda) = \nabla_{\lambda} \mathbb{E}_q[j(\theta)] = \mathbb{E}_q[j(\theta) \nabla_{\lambda} \log q(\theta; \lambda)] \quad (\text{G.5})$$

$$G^{\text{score}}(\lambda) = \mathbb{E}_q[\Delta_{\mu}^{\text{score}}] \quad (\text{G.6})$$

$$\Delta_{\mu}^{\text{score}}(\text{KL}(q||p)) = \theta^2(\theta - \mu) \quad (\text{G.7})$$

$$\mathbb{V}_q(\Delta_{\mu}^{\text{score}}(\theta; \lambda)(\mu))(\text{KL}(q||p)) = \mu^4 + 14\mu^2 + 15 \quad (\text{G.8})$$



Now consider the score gradient for Inclusive KL and  $\alpha$  divergences:

$$G_\alpha^{\text{score}}(\lambda) = \mathbb{E}\left[\frac{p(Y, \theta)^\alpha}{q(\theta)} \nabla_\lambda \log q(\theta_s; \lambda)\right] \quad (\text{G.9})$$

Taking the target density,  $p(Y, \theta) = -\theta^2/2$ , where the factor  $1/2$  helps in cancelling some terms. For the special case,  $q(\theta) = N(\mu, 1)$ , when  $\mu = 0$ , the two densities become equal and we are left only with  $G_\alpha^{\text{score}}(\lambda) = \theta$ . Then, but for a general case this is given as:

$$G_\alpha^{\text{score}}(\lambda) = \mathbb{E}\left[\frac{\exp(-\theta^2/2)}{\exp(-(\theta - \mu)^2/2)} \nabla_\lambda \log q(\theta_s; \lambda)\right] \quad (\text{G.10})$$

$$= \mathbb{E}_q[\exp(\mu^2/2 + \theta\mu)^\alpha \nabla_\lambda \log q(\theta_s; \lambda)] \quad (\text{G.11})$$

For the special case when  $\alpha \rightarrow 1$ , we get

$$G_\alpha^{\text{score}}(\lambda) = \exp(\mu^2/2) \mathbb{E}_q[\exp(\theta\mu)(\theta - \mu)] \quad (\text{G.12})$$

$$\mathbb{V}(\Delta_\mu^{\text{score}}) = \exp(\mu^4/4) \mathbb{V}_q[\exp(\theta\mu)(\theta - \mu)] \quad (\text{G.13})$$

when  $\mu = 0$ , meaning that the approximation is same as the target density, this reduces to  $\mathbb{V}_q(\Delta_\mu^{\text{score}}(\theta; \lambda)(\mu)) = 1$  (a constant), equal to the variance of a standard normal distribution.